CX3CL1 Promotes Breast Cancer via Transactivation of the EGF Pathway

Manuel Tardáguila[1], **Emilia Mira**[1], **Miguel A. García-Cabezas**[2], **Anna M. Feijoo**[1], **Miguel Quintela-Fandino**[3], **Iñigo Azcoitia**[4], **Sergio A. Lira**[5], and **Santos Mañes**[1]

[1]Department of Immunology and Oncology, Centro Nacional de Biotecnología/CSIC

[2]Department of Anatomic Pathology, Hospital Universitario La Paz

[3]Breast Cancer Unit, Clinical Research Program CNIO-Spanish National Cancer Research Center

[4]Cell Biology, Faculty of Biology, Universidad Complutense de Madrid, Madrid, Spain

[5]Immunology Institute, Icahn School of Medicine at Mount Sinai, New York, New York

Abstract

Chemokines are relevant molecules in shaping the tumor microenvironment, although their contributions to tumorigenesis are not fully understood. We studied the influence of the chemokine CX3CL1/fractalkine in *de novo* breast cancer formation using HER2/*neu* transgenic mice. CX3CL1 expression was downmodulated in HER2/neu tumors, yet, paradoxically, adenovirus-mediated CX3CL1 expression in the tumor milieu enhanced mammary tumor numbers in a dose-dependent manner. Increased tumor multiplicity was not a consequence of CX3CL1-induced metastatic dissemination of the primary tumor, although CX3CL1 induced epithelial-to-mesenchymal transition in breast cancer cells *in vitro*. Instead, CX3CL1 triggered cell proliferation by induction of ErbB receptors through the proteolytic shedding of an ErbB ligand. This effect was important insofar as mammary tumorigenesis was delayed and tumor multiplicity was reduced by genetic deletion of CX3CL1 in HER2/neu mice, but not in polyoma middle T-antigen oncomice. Our findings support the conclusion that CX3CL1 acts as a positive modifier of breast cancer in concert with ErbB receptors.

Corresponding Author: Santos Mañes, Centro Nacional de Biotecnología, Darwin, 3, Campus Cantoblanco, Madrid 28049, Spain. Phone: 34-91 585-4840; Fax: 34-91-372-0493; smanes@cnb.csic.es.

Disclosure of Potential Conflicts of Interest

No potential conflicts of interest were disclosed.

Authors' Contributions

Conception and design: M. Tardaguila, S. Mañes

Development of methodology: E. Mira

Acquisition of data (provided animals, acquired and managed patients, provided facilities, etc.): M. Tardaguila, A.M. Feijoo, M. Quintela-Fandino, I. Azcoitia, S.A. Lira

Analysis and interpretation of data (e.g., statistical analysis, biostatistics, computational analysis): M. Tardaguila, E. Mira, M.A. García-Cabezas, I. Azcoitia

Writing, review, and/or revision of the manuscript: M. Tardaguila, E. Mira, M. Quintela-Fandino, S.A. Lira, S. Mañes

Administrative, technical, or material support (i.e., reporting or organizing data, constructing databases): M. Quintela-Fandino

Study supervision: S. Mañes

Note: Supplementary data for this article are available at Cancer Research Online (http://cancerres.aacrjournals.org/).

Introduction

The development of most solid tumors is intimately linked to external cues provided by the microenvironment (1). Based mainly on associative studies in human cancers and tumor transplant models, a family of chemotactic proteins termed chemokines has emerged as important molecular regulators of carcinogenesis by shaping the tumor milieu. Most established human tumors produce chemokines, and their expression is associated with poor prognosis (2). The protumor effects correlate with direct activity on cancer cells as well as with the regulation of leukocyte and mesenchymal stem cell trafficking into the tumor, which create inflammatory conditions that promote progression of premalignant lesions into malignant neoplasms (2, 3). Nonetheless, specific chemokines can also exert antitumor effects by fostering immune responses that eliminate tumor cells (4, 5) and/or by inhibiting cell transformation and proliferation (6, 7). These paradoxical results suggest that chemokine function in tumor biology is likely to be tissue- and cell context-dependent. Moreover, the integration of chemokine cues with the complex array of other signals in the tumor environment is usually underestimated. The development of preclinical models that closely recapitulate the evolution of human malignancies would help to clarify the impact of specific chemokines on the biology of individual tumor types.

In a pilot screening for chemokine/chemokine receptor expression in various human primary cancers, we found that CX3CL1, also termed fractalkine, was downmodulated specifically in breast carcinomas compared with adjacent normal tissue (unpublished data). This prompted us to study this chemokine and its receptor, CX3CR1, in more detail in breast carcinogenesis.

CX3CR1 expression is reported in different types of cancer cell lines (8, 9), including those from the breast (10), where it transduces CX3CL1-induced signals involved in phosphoinositide 3-kinase (PI3K)-mediated survival, proliferation and metastases. In apparent contradiction, CX3CL1 is a transcriptional target of TP53 (11), suggesting CX3CL1/CX3CR1 involvement in tumor suppression. Moreover, forced CX3CL1 expression by tumor cells enhances NK- and CD8^{+} T lymphocyte–mediated antitumor immunity (12–14). Although these associative studies in human cancers and graft models show a role for CX3CL1/CXC3R1 in tumor biology, to our knowledge, no reports have shown an indispensable role for this pair in spontaneous carcinogenesis.

We addressed this question using transgenic FVB/N-Tg (MMTVneu) mice (Tg-neu), which overexpress the protooncogene *neu* (the rat *erbB2* ortholog) under the control of the murine mammary tumor virus (MMTV) LTR; these Tg-neu mice develop spontaneous mammary tumors in a stepwise manner, similar to that seen in human ErbB2^{+} breast tumors. Increased Her2/ErbB2/Neu expression and activation is linked to the initiation and progression of human cancers, particularly in the breast (15). ErbB2 tyrosine kinase receptor (RTK) does not bind any known ligand, but amplifies signaling of other ligand-occupied receptors of the same family, Her1/ ErbB1/EGFR (EGF receptor), Her3/ErbB3, and Her4/ErbB4. There are 11 stimulatory ligands, some of which are expressed as membrane-anchored precursors, with distinct receptor specificity and affinity (16). These ligands trigger homo- and heterodimerization of ErbB receptors, leading to tyrosine phosphorylation and signal

transduction; heterodimerization even enables signaling of the kinase-defective receptor ErbB3.

ErbB receptors can be modulated indirectly by a broad set of heterologous receptors in response to environmental conditions. Cytokine receptors, voltage-gated Ca^{2+} channels, integrins, G protein-coupled receptors (GPCR), and Wnt signals induce ErbB receptor transactivation (17, 18). In some cases, this crosstalk involves direct transphosphorylation by intracellular tyrosine or serine/threonine kinases, causing ErbB receptor activation or endocytosis, respectively (19, 20). In many cases, the crosstalk involves cleavage of a transmembrane EGF-like precursor, which then activates the receptor in a paracrine/autocrine manner (18, 21); this seems to be the mechanism by which CX3CL1 induces ErbB1 transactivation in smooth muscle cells (22). Transactivation of ErbB receptors could contribute to cancer by integrating distinct signals in the tumor milieu (17).

Using gain- and loss-of-function approaches, we provide genetic evidence that supports a role for CX3CL1 in mammary carcinoma promotion in Tg-neu mice. CX3CL1 transactivates ErbB receptors in human breast cancer cells and Tg-neu mouse primary mammary gland cultures, leading to the induction of the ERK pathway and cell proliferation. In contrast, CX3CL1 does not influence mammary carcinogenesis in Tg-PyMT mice, in which the ERK signaling pathway is constitutively activated by the mouse polyoma virus middle T-antigen (PyMT) oncogene. We thus propose that CX3CL1 acts as a specific tumor promoter for ErbB2-expressing mammary carcinomas.

Materials and Methods

Mouse and human samples

Transgenic FVB/N-Tg(MMTV-neu)202Mul/J mice and transgenic MMTV-polyoma middle T-antigen (FVB/N-Tg (MMTV-PyVT)634Mul/J) mice were from Jackson Laboratory. C57BL/6 CX3CL1$^{-/-}$ mice (23) were backcrossed for more than 10 generations to the FVB background while maintaining CX3CL1 in heterozygosis. CX3CL1$^{+/+}$ (WT), CX3CL1$^{+/-}$, and CX3CL1$^{-/-}$ littermates on Tg-neu or Tg-PyMT backgrounds were generated after crossing appropriate heterozygous mice, and were monitored weekly for mammary tumors from age 20 (neu) or 4 weeks (PyMT). When detected, tumors were measured weekly with calipers and volume calculated (24). Live animal experiments were supervised by the Centro Nacional de Biotecnología Ethics Committee according to national and European Union guidelines.

To study for human breast tumors, we used 4 samples (2 intraductal and 2 invasive breast carcinomas), obtained from the Spanish Centro Nacional de Investigaciones Oncológicas (CNIO) Tumor Biobank (Madrid, Spain), a national network with anonymized patient data that coordinates the main hospitals in Spain. Institutional ethics boards approved sample transfer to local biobanks with patient consent. All 4 cases (all HER-2-positive) were derived from primary breast surgery for suspicion of malignancy based on radiologic findings.

Cell lines

MCF-10A, T47D, MCF-7, BT-474, MDA-MB-468, Hs-578T, and MDA-MB-231 were from the American Type Culture Collection. Murine N202.1A and 1g11 cell lines were kind gifts from V. Bronte (Verona University, Verona, Italy) and A. Mantovani (Inst. Humanitas, Milan, Italy), respectively. Cells were cultured in distinct media (Supplementary Table S1) supplemented with 2 mmol/L glutamine and 100 U/mL each penicillin and streptomycin. MDA-MB-468 cells were cultured at 37° C in air without supplementary CO_2.

Isolation of cell subpopulations from mammary glands and tumors

Mammary glands were extracted from Tg-neu mice (8- to 12-week-old) after removal of inguinal lymph nodes. For mammary tumors, a single tumor mass was used in each experiment. Glands and tumors were digested (16 hours, 37° C) in Dulbecco's Modified Eagle Media (DMEM)/F12 (1:1) with 300 U/mL collagenase/100 U/mL hyaluronidase (Stem Cell Technologies) and gentamycin (50 μg/mL). Digestion was terminated by addition of HBSS (Gibco) with 10 mmol/L HEPES and 2% fetal calf serum (FCS), and single-cell suspensions obtained (25). CD45^{+} and ER119^{+} cells were depleted by sequential incubation with anti-CD45 (clone 30-F11) and -TER119 (TER119; BD Biosciences), followed by sheep-anti-rat–coated magnetic beads (Invitrogen). Remaining cells were stained with anti-CD31-PE (MEC 13.3) and -CD24-FITC (M1/69; BD Biosciences) antibodies and sorted by FACS (Beckman Coulter). Isolated fractions were lysed immediately with TRI Reagent (Sigma) and stored (−80°C) for RNA extraction. Samples of each isolation stage were stained with the violet Live/Dead Cell Stain Kit (Invitrogen) and anti-CD45-FITC (I3/2.3), CD31-PE, and CD24-PE-Cy5 (BD Biosciences).

Quantitative PCR

Murine and human CX3CR1 and CX3CL1 were quantified by quantitative real-time PCR (qRT-PCR), using the primers listed in Supplementary Table S2, in an ABI PRISM 7900 HT using SYBR Green-based reaction mix (Euroclone) and β-actin to normalize data. The first cDNA strand was synthesized from total RNA (usually 1 μg) with the High-Capacity cDNA Archive Kit (Applied Biosystems) using random octamers as primers. Melting curve analyses were conducted to validate generation of the specific PCR product.

CX3CL1 ELISA

CX3CL1 concentration was measured in extracts, serum, or culture supernatants with Human or Mouse CX3CL1 DuoSet ELISA (R&D Systems), with plates coated with capture antibody (4°C, overnight). Breast tumors or glands were dissected from Tg-neu mice, pulverized in liquid N_2, and the powder homogenized in radioimmunoprecipitation assay (RIPA) buffer with protease and phosphatase inhibitors. Protein in cleared homogenate (20,000 × *g*, 30 minutes) was quantified (micro-BCA Protein Assay Kit, Pierce) and aliquoted (−80° C). Different amounts of total protein were assayed in triplicate for each sample; nonspecific signal was determined in each experiment by assaying an extract from pooled mammary glands of CX3CL1^{−/−} mice, and subtracted from each sample value. Human and mouse cell lines were lysed in RIPA buffer and extracts assayed as above.

Adenoviral gene therapy

The AdEasy Adenoviral Vector System (Stratagene) was used throughout. Murine CX3CL1 cDNA was amplified and cloned into the shuttle pCMV vector. High titer stock of Ad-CX3CL1 and Ad-LacZ were prepared by the Unidad de Producción de Vectores (Centro de Biotecnología Animal y Terapia Génica, Barcelona, Spain). Ad-CX3CL1 and Ad-LacZ virus activity was analyzed by infection of N202.1A and 1g11 cells in solution; CX3CL1 levels and β-galactosidase activity were measured after 72 hours. For mouse studies, Ad-CX3CL1 or Ad-LacZ viruses (5×10^8 infective particles/40 μL) were injected into Tg-neu mouse tumors (75–150 mm^3) at a single dose or in six doses (two per week). Injected tumors were measured weekly and mice monitored for new lumps. Histopathologic analyses were conducted on hematoxylin/eosin-stained sections of tumors, healthy mammary glands, and axillary, cervical, and inguinal lymph nodes of treated mice; several representative sections of each sample were analyzed.

Epithelial-to-mesenchymal transition assays

CX3CL1-induced expression of *snail-1, snail-2, twist-1* and *cdh1* (E-cadherin) genes was studied in Ad-CX3CL1- and Ad-LacZ- infected [100 multiplicity of infection (MOI)] T47D cells (80%–90% confluence) by qRT-PCR using specific primers (26). In some cases, T47D-infected cells (48 hours after infection) were treated (24 hours, 37° C) with PTx (750 ng/mL, Sigma) or vehicle.

For subcellular E-cadherin location studies, T47D cells were seeded on fibronectin-coated slides, pretreated (8 hours, 37°C) with PBS or CX3CL1$^{29–102}$ antagonist (R&D Systems), and stimulated with CX3CL1 (11 nmol/L; 24 hours, 37°C). Cells were fixed (4% paraformaldehyde), permeabilized (0.1% Triton X-100), and stained sequentially with anti-E-cadherin (Sigma) and Alexa488-anti-mouse antibody (Jackson ImmunoResearch). Samples were mounted in Vectashield/DAPI medium (Vector Laboratories); images were acquired with a LSM 510 Meta confocal microscope (Zeiss) and processed with ImageJ.

Cell migration was assayed in vitronectin-coated (5 μg/mL, 20 hours, 4° C; BD Biosciences) Transwell chambers (8 μm pore; Costar). T47D cells were pretreated (24 hours) with CX3CL1 (30 nmol/L) in RPMI with 0.1% bovine serum albumin (RPMI-BSA), washed extensively, and seeded (10^5 cells) in the top chamber; bottom chambers were filled with RPMI-BSA alone or with 1% FCS, CX3CL1, or both. After incubation (18 hours, 37° C), cells on the top side of the membrane were removed with a cotton swab, and cells on the underside were fixed and stained (Grifols Staining Solution, Spain). Cells were counted in six different high-power fields in triplicate wells, in two independent experiments.

[^{3}H]-thymidine incorporation assays

T47D cells (10^4 well) were pretreated (1 hour, 37° C) with matrix metalloproteases (MMP) inhibitors AG1478 or GM6001 (both at 1 μmol/L), stimulated with CX3CL1 (60 nmol/L; 36 hours), and pulsed with methyl-[^{3}H]-thymidine ([^{3}H]-TdR, 1 μCi/well, 12 hours; Perkin Elmer). Nuclei were harvested using a MicroBeta TriLux workstation and [^{3}H]-TdR incorporation was determined on a liquid scintillation counter (Perkin Elmer).

CX3CL1-induced signaling

Serum-starved (48 hours) T47D cells were pretreated with PTx (750 ng/mL, 16 hours), AG1478 (1 μmol/L, 1 hour; Calbiochem) or GM6001 (1 μmol/L, 1 hour; Chemicon) and stimulated with CX3CL1 (30 nmol/L) or EGF (10 ng/mL) for indicated times. Cells were lysed in ice-cold 20 mmol/L Tris-HCl pH 7.0, 140 mmol/L NaCl, 50 mmol/L EDTA, 1% glycerol, 1% NP-40, with protease and phosphatase inhibitors. Protein lysates (20 μg) were resolved in SDS-PAGE and blotted with polyclonal antibodies to the unphosphorylated and phosphorylated forms of extracellular regulated kinases (ERK-1/2) and AKT (Cell Signaling Technology). Blots were stripped in Reblot Plus Strong Solution (15 minutes, 20° C; Millipore). In blocking experiments, T47D cells were pretreated (10 minutes, 37°C) with neutralizing antibodies (20 μg/mL; R&D Systems) to human amphiregulin (MAB262), HB-EGF (AF-259), TGFα (AF-239), or nonspecific IgG, before stimulation with CX3CL1 (as above) or appropriate ligands.

For immunoprecipitation, cells were lysed in ice-cold Tris buffer as above but containing 0.5% NP-40, and further disrupted by sonication. Cell lysates (0.5 mg) were precleared with goat anti-mouse IgG antibody coupled to agarose beads (Sigma) before incubation (1 hour, 4°C) with agarose-coupled anti-phosphotyrosine (pTyr) monoclonal antibody (clone PY69; BD Biosciences). Immunoprecipitates were assayed by Western blot analysis with anti-EGFR (D38B1) and -HER-2 (29D8) antibodies (Cell Signaling Technology).

Calcium mobilization assays were conducted as described (27). Serum-starved (48 hours) T47D cells, untreated or pretreated with PTx (750 ng/mL), were loaded with Fluo-3,AM (300 mmol/L, 20 minutes, 37° C; Molecular Probes). Cells were prewarmed in RPMI-BSA with 2 mmol/L $CaCl_2$ before CX3CL1 stimulation (60 nmol/L). Ca^{2+}release was determined (37° C, 525 nm) in an EPICS XL cytometer (Beckman Coulter).

For primary cultures, CD45- and Ter119-depleted cell suspensions were cultured (20 hours) in EpiCult-B (Stem Cell Technologies) with 5% FCS and gentamycin, followed by starvation in DMEM:F12 (1:1) with 0.5% FCS (4 hours), and then stimulated with recombinant murine CX3CL1 (200 nmol/L; R&D Systems). Cell extracts were assayed by Western blot analysis with polyclonal anti-pErbB2 (Upstate Biotechnology) and -HER-2 (29D8).

Immunohistochemistry

CX3CL1 was analyzed in cryosections of mouse mammary glands, blocked with 10% BSA in PBS (2 hours, 20°C), followed by incubation (16 hours, 4°C) with anti-CX3CL1 antibodies AF537 (2 μg/mL) or MAB571 (1.1 μg/mL; both from R&D Systems), or sc-7227 (8 μg/mL; Santa Cruz Biotechnology). After incubation with appropriate secondary antibodies (1 hour, 20° C), samples were mounted and observed under a fluorescence microscope (Leica). CX3CR1 was analyzed in mammary tumors and glands using a recombinant hFc-CX3CL1 prepared in our laboratory, followed by biotin-rat anti-hFc antibody and Cy3-streptavidin. Paraffin-embedded human breast carcinomas were stained with the anti-CX3CL1 antibody AF365 (R&D Systems; 15 μg/mL, 14 hours, 4° C) in PBS containing 1.5% rabbit serum. After incubation with a biotin-labeled rabbit anti-goat

antibody (1 hour, 20° C) and amplification with the ABC method (Thermo Scientific), the signal was developed with 3-amino-9-ethylcarbazole (Sigma-Aldrich). Sections were hematoxylin-counterstained.

Statistical analysis

Significant differences were identified by Student t test, Mann–Whitney test, one-way ANOVA with Dunnett posttest, two-way ANOVA with Bonferroni posttest, and a Fisher two-tailed test, as indicated. Data are expressed as mean ± SEM.

Results

CX3CL1/CX3CR1 are expressed in the mammary gland

Although CX3CL1/CX3CR1 are implicated in oncogenesis in several tissues, the expression and function of this pair in spontaneous carcinogenesis has not been analyzed. We combined magnetic isolation and flow cytometry to analyze CX3CL1 mRNA expression in cell subpopulations from mammary glands before tumor onset in Tg-neu mice. Five major cell populations were isolated based on 3 markers, CD45 (leukocytes), CD31 (endothelial cells), and CD24, which distinguishes luminal epithelial cells (CD24^{high}), basal/myoepithelial cells (CD24^{med}), and a mixed CD24$^{low/-}$ population composed of fibroblasts, adipocytes, and neurons (25, 28). A representative isolation experiment is shown (Fig. 1A) as well as the relative proportion of each cell type in mammary gland (Fig. 1B). Endothelial and epithelial cells expressed CX3CL1 mRNA; in epithelial cells, expression was higher in luminal (CD24^{high}) than in basal/myoepithelial cells (CD24^{med}) (Fig. 1C). Hematopoietic cells showed no CX3CL1 mRNA, but expressed the highest levels of its receptor, CX3CR1, compared with endothelial and luminal epithelial cells (Fig. 1C and D). CX3CR1 mRNA was undetectable in CD24^{med} and CD24$^{low/-}$ cells. Attempts to visualize CX3CL1 by immunohistochemistry in mammary glands of nulliparous Tg-neu mice before tumor onset were unsuccessful, as three commercial antibodies yielded similar erratic staining in mammary tissue from wild-type and CX3CL1$^{-/-}$ mice (Supplementary Fig. S1).

CX3CL1 is downmodulated in breast tumors

We tested CX3CL1/CX3CR1 expression after mammary tumor onset. Most cells isolated from these tumors were CD24^{high}, which is consistent with the luminal origin of Tg-neu mammary carcinomas; some endothelial and hematopoietic cells also infiltrated these tumors (Fig. 2A). Only endothelial and luminal epithelial cells expressed CX3CL1. CX3CL1 mRNA levels were significantly downmodulated in CD24^{high} tumor cells compared with untransformed cells (Fig. 2B); CX3CL1 mRNA was also slightly reduced in endothelial cells isolated from tumors relative to normal tissue. CX3CL1 protein levels were lower in total extracts from tumors versus normal mammary tissue (Fig. 2C); paired analysis of CX3CL1 levels in tumors and healthy mammary glands from the same mice confirmed CX3CL1 downmodulation in carcinomas (Fig. 2D).

In contrast, CX3CR1 mRNA was upregulated in specific cell populations isolated from tumors; this increase was significant in CD24^{high} and CD45$^+$ cells, but receptor expression was unaffected in endothelial cells (Fig. 2E). Fc-CX3CL1 staining showed CX3CR1

expression in tumors and in normal mammary tissue (Supplementary Fig. S2); differences in staining intensity between the two tissues were not evident, as would be predicted by mRNA data.

We analyzed CX3CL1 and CX3CR1 regulation in human breast tumors. Analysis of public data (GEOprofile Database GSE3744, GDS3324; EMBL-EBI Database GEOD10780) from three independent studies (29–31) showed downregulation of CX3CL1 expression in human primary breast tumors compared with healthy breast tissue (Fig. 2F). The results for CX3CR1 were not conclusive, as only two of these studies showed a significant reduction in CX3CR1 mRNA in tumor samples (Fig. 2F). CX3CL1 staining was lower in a small set of *in situ* and invasive human breast ductal carcinomas compared with nontumor tissue from the same patient (Fig. 2G and H). Downmodulation of CX3CL1 expression in Tg-neu tumors might thus be a broad phenomenon in human breast cancer.

CX3CL1 overexpression increases tumor number in Tg-neu mice

Given the antitumor activity of CX3CL1 in some cancer models (12–14, 32), its downregulation in Tg-neu tumors could be the result of a selection mechanism that silences a potential antioncogenic factor. CX3CL1 is produced as a membrane-anchored protein that can be cleaved by specific MMPs; tethered and shed CX3CL1 forms can have different functions (33, 34). To assess the result of enhanced CX3CL1 expression in the tumor environment, we inoculated Tg-neu mice intratumorally with recombinant adenoviruses to express the full-length (membrane-tethered) CX3CL1 (Ad–CX3CL1) or β-galactosidase (Ad-LacZ). These adenoviruses infected the N202.1A murine mammary cancer cell line (Fig. 3A and B) and the 1g11 mouse endothelial cell line (Fig. 3C and D), as determined by dose-dependent expression of CX3CL1 mRNA and protein; β-galactosidase activity was also detected in extracts of Ad–LacZ–infected N202.1A cells (Fig. 3B). These adenoviruses thus transduce the *cx3cl1* gene in various cell types in the tumor parenchyma.

As soon as Tg-neu mice presented a palpable lump (75–150 mm^3), they received six intratumoral injections of Ad-CX3CL1 or Ad-LacZ. As predicted, Ad-CX3CL1 intratumoral injection increased CX3CL1 mRNA levels in tumor (CD24^{+}) and endothelial (CD31^{+}) cells (Fig. 3E), as well as serum CX3CL1 levels (Fig. 3F) compared with those in Ad-LacZ–injected mice. Primary tumors that received injections of Ad-CX3CL1 and Ad–LacZ had similar growth kinetics (Fig. 3G), and showed no relevant differences in morphology, malignancy score, or mitotic figures (Fig. 3H and I); the tumors were noninfiltrating. Proliferation and apoptosis rates, determined by phosphohistone H3 and TUNEL staining, respectively, were also comparable for Ad-LacZ- and Ad-CX3CL1–treated tumors (Supplementary Fig. S3A and S3B). There were no apparent differences in the angiogenic pattern between the two tumor groups (Supplementary Fig. S3C).

Ad-CX3CL1–treated mice showed a significant increase in the number of mammary glands with palpable tumors compared with those treated with Ad-LacZ (Fig. 3J). Moreover, mammary glands from treated mice with no macro-scopically detectable tumors exhibited microscopic tumors composed of epithelial cells with moderate atypia and some mitoses (Fig. 4A and B); these masses did not invade the surrounding stroma and showed no sign of necrosis. Some acini and ductuli near these tumors had normal structure (Fig. 4C), whereas

others showed proliferation towards the lumen of epithelial cells with mild atypia (Fig. 4D); hyperplastic foci were not always found in the vicinity of tumors (Fig. 4E). These microscopic tumors were more abundant in Ad-CX3CL1- than in Ad-LacZ–injected mice; of six mammary glands analyzed in each case, we detected five foci in Ad-CX3CL1- and two in Ad-LacZ–treated mice. To analyze whether differences in tumor multiplicity between adenoviruses were due to a LacZ-induced immune response, CD4^{+} or CD8^{+} T cells were isolated from lymph nodes and spleen of Ad-CX3CL1- (control) and Ad-LacZ– injected mice, and incubated *ex vivo* with syngeneic, γ-irradiated splenocytes loaded with 50, 5, or 0.5 µg of LacZ. Proliferation of T cells from Ad-LacZ- or Ad-CX3CL1– injected mice showed no differences at any antigen dose tested (data not shown), suggesting that repeated intratumoral Ad-LacZ injection did not induce a specific T-cell response in our mice.

We also observed a tendency toward increased multiplicity of palpable tumors in mice that received a single intartumoral dose of Ad-CX3CL1, although tumor growth kinetics were unaffected (Supplementary Fig. S4). Elevation of CX3CL1 levels in the tumor environment seems to promote mammary carcinogenesis in Tg-neu mice in a manner dependent on dose and/or duration of exposure.

Lack of lymph node metastases in Ad-CX3CL1-injected mice

As CX3CL1 can induce metastasis in some models (8, 9), the Ad-CX3CL1-induced increase in tumor multiplicity could be a result of neoplastic cell dissemination due to chemokine overexpression. Analysis of a collection of human breast cancer cell subtypes with distinct metastatic capacity (35) showed no apparent correlation between CX3CL1 or CX3CR1 mRNA (Supplementary Fig. S5) or protein expression (Supplementary Fig. S6) and the invasive/metastatic potential of the cell lines tested; the untransformed breast epithelial cell line MCF-10A was used as a reference. We also tested whether CX3CL1 could induce epithelial-to-mesenchymal transition (EMT) in breast cancer cells, as EMT is proposed as a central step in breast cancer dissemination (36, 37). T47D cells, which express CX3CR1 but not its ligand, were infected with Ad–CX3CL1 and Ad-LacZ. Ad-CX3CL1–infected cells showed significantly upregulated mRNA levels of the EMT master gene *snail2* (formerly *slug*) compared with Ad-LacZ–infected cells (Supplementary Fig. S7A). Increased *snail2* expression in Ad-CX3CL1 cells was pertussis toxin (PTx)-sensitive (Supplementary Fig. S7B), indicating that this upregulation was $G\alpha_i$-mediated. Moreover, CX3CL1 stimulation delocalized E-cadherin from intercellular membranes of T47D cells; this phenotype was partially reversed by coincubation of CX3CL1 with the N–terminal truncated antagonist CX3CL1[29–102] (Supplementary Fig. S7C–S7E). CX3CL1-induced delocalization of intercellular E-cadherin correlated with the dose-dependent effect of CX3CL1 in boosting serum-induced T47D cell migration (Supplementary Fig. S7F). The lymphatic vessels are most common route of initial tumor cell dissemination *in vivo* (38). Although CX3CL1 induced EMT and enhanced cancer cell motility *in vitro*, we found no tumor cells in axillary, cervical, or inguinal lymph nodes from Ad-CX3CL1- (*n* = 24) or Ad-LacZ–injected mice (*n* = 18; Supplementary Fig. S8). We detect no tumor cells in blood or metastases in lung.

CX3CL1 induces transactivation of the EGF pathway

An alternative explanation for the increased tumor multiplicity in Ad-CX3CL1-injected mice is the CX3CL1 potential to stimulate tumor cell expansion, which we studied using T47D cells. [^{3}H]-TdR incorporation assays showed that CX3CL1 alone was a weak mitogen; nevertheless, it enhanced cell proliferation in the presence of FCS (Fig. 5A). CX3CL1-induced T47D cell proliferation was inhibited by treatment with AG1478, an inhibitor of ErbB1 kinase activity, or the broad-spectrum MMP inhibitor GM6001 (Fig. 5A). These results suggested that CX3CL1-induced T47D cell proliferation involves transactivation of ErbB receptors through MMP-dependent shedding of a transmembrane ligand precursor of the EGF axis, as reported for other cell types (22)

To obtain direct evidence that CX3CL1 activates the EGF pathway, we analyzed tyrosine phosphorylation of ErbB receptors in CX3CL1-stimulated T47D cells. These cells express ErbB receptor levels comparable with those in normal breast tissue and do not show ErbB2 amplification (data not shown). In this model, CX3CL1 induced ErbB1 phosphorylation, which peaked at 10 to 30 minutes after stimulation (Fig. 5B); AG1478 abrogated CX3CL1-induced ErbB1 phosphorylation, indicating that it required the ErbB1 kinase activity (Fig. 5B).

We then tested the dependence of CX3CL1-triggered signaling pathways on ErbB transactivation. PTx treatment inhibited CX3CL1-mediated Ca^{2+} flux (Fig. 5C), implicating a G$_i$ protein in this process. In contrast, CX3CL1-induced ERK1/2 phosphorylation was unaffected by PTx, but was significantly reduced after GM6001 or AG1478 treatment (Fig. 5D and Supplementary Fig. S9A), suggesting the importance of CX3CL1/ErbB crosstalk in the activation of the mitogenic ERK pathway. Neither PTx nor the MMP inhibitors GM6001 or BB94 inhibited AKT phosphorylation (Fig. 5E and Supplementary Fig. S9B), implying that it is independent of ErbB transactivation. It should be noted that T47D cells have mutations in the PI3K pathway (39).

T47D cells express several membrane-bound EGF family ligands (Supplementary Fig. S10). To determine which of these ligands is involved in CX3CL1/ErbB crosstalk, T47D cells were stimulated with CX3CL1 in the presence of neutralizing anti-bodies to amphiregulin, HB-EGF, or TGFα. Each of these antibodies partially inhibited CX3CL1-induced ERK1/2 phosphorylation (Fig. 5F), suggesting that multiple ErbB ligands are involved in the transactivation circuit.

To determine whether CX3CL1-induced ErbB activation occurs in primary Tg-neu tumors, we stimulated cells from spontaneous carcinomas with CX3CL1, alone or with GM6001, to prevent proteolysis of EGF precursors; phosphorylated ErbB2 levels were then analyzed in total cell extracts. CX3CL1 stimulation of primary tumor cells induced only a slight increase in ErbB2 phosphorylation, which was not inhibited by GM6001 (Fig. 5G), possibly due to constitutive ErbB2 phosphorylation in the Tg-neu model (Fig. 5G; ref. 40). We therefore analyzed CX3CL1/ErbB crosstalk in primary mammary epithelium, before transforming ErbB2 mutations occurred. CX3CL1 stimulation of these cultures induced a clear increase in ErbB2 phosphorylation, which was inhibited by GM6001 addition (Fig. 5H). These data

thus indicated that CX3CL1 triggers ErbB2 transactivation in the preneoplastic mammary epithelium of Tg-neu mice.

CX3CL1 deficiency delays mammary tumor onset in Tg-neu mice

One implication of these results is that CX3CL1 deficiency would affect mammary tumorigenesis in Tg-neu mice. We crossed C57BL/6-CX3CL1$^{-/-}$ with Tg-neu mice; as C57BL/6-FVB/N-Tg(MMTVneu)-CX3CL1$^{-/-}$ mice were extremely resistant to mammary cancer (data not shown), we backcrossed mice for more than 10 generations on the FVB background. Although C57BL/6–CX3CL1$^{-/-}$ mice show no overt phenotype (23), approximately 60% of FVB-Tg-neu-CX3CL1$^{-/-}$ mice died of causes that remain to be identified; death was not sex-associated. CX3CL1 deficiency did not compromise mammary gland development or architecture, as suggested by the lack of lactation problems in the surviving Tg-neu-CX3CL1$^{-/-}$ mice and the lack of differences in the structure and cell types composing the mammary gland of mature Tg-neu-CX3CL1$^{-/-}$ compared with wild-type (WT) mice (Supplementary Fig. S11).

Analysis of nulliparous Tg-neu-CX3CL1$^{-/-}$ mice showed a significant delay in mammary tumor onset (Fig. 6A) and decreased tumor multiplicity (Fig. 6B) compared with WT mice. Approximately 30% of Tg-neu-CX3CL1$^{-/-}$ females had not developed tumors by 15 months of age. Tg-neu-CX3CL1 mice also showed a significant delay in tumor onset (Fig. 6A) and a decrease in tumor multiplicity (Fig. 6B) compared with WT controls. It should be noted that CX3CL1 expression was hemizygous in Tg-neu-CX3CL1$^{+/-}$ mouse mammary tissue and tumors (Supplementary Fig. S12). Tumors in all three genotypes showed no differences in growth kinetics (Fig. 6C), again suggesting CX3CL1 involvement only at early stages of mammary carcinogenesis.

The delayed onset and reduced number of mammary tumors in CX3CL1-deficient and hemizygous mice might be linked to the crosstalk between this chemokine and ErbB2. FVB-Tg(MMTV-PyMT) (Tg-PyMT) mice develop multifocal, aggressive polyclonal tumors at 7 to 8 weeks of age, due to PyMT activation of a number of signaling molecules, many of which are shared with ErbB2 (41). We generated CX3CL1-deficient Tg-PyMT mice; Tg-PyMT-CX3CL1$^{-/-}$, -CX3CL1$^{+/-}$, and WT mice showed no difference in tumor onset (Fig. 6D) or in mean tumor number per mouse (Fig. 6E). Tumor growth kinetics were similar for Tg-PyMT-CX3CL1$^{+/-}$ and WT mice, with a slight reduction in Tg-PyMT-CX3CL1$^{-/-}$ mice at late stages (Fig. 6F). These results suggest that the mammary carcinogenesis inhibition associated with reduced CX3CL1 levels depends on ErbB2 overexpression.

Discussion

Several *in vitro* and transplantable tumor model studies have analyzed the influence of the CX3CL1/CX3CR1 pair in the biology of tumor cells and the possible use of targeting CX3CL1 for immunotherapy. Here, we studied CX3CL1 and CX3CR1 expression in the mammary gland and in spontaneous mammary carcinogenesis.

In Tg-neu mice, mammary tumors showed increased CX3CR1 and decreased CX3CL1 mRNA levels compared with healthy tissue. Despite CX3CL1 downregulation in established

tumors, our data suggest that CX3CL1 is a tumor promoter in Tg-neu mice. Two lines of evidence support this hypothesis. First, ectopic CX3CL1 expression by Ad-CX3CL1 injection increased tumor multiplicity, although it did not affect tumor growth kinetics. In *in vitro* studies, Ad-CX3CL1 elicited changes in gene expression reminiscent of EMT in T47D breast cancer cells, and potentiated migration of these cells, suggesting a "permissive" role for CX3CL1 in cancer cell motility, as described for CCL5 (42). *In vivo* results nonetheless indicated that Ad-CX3CL1 did not induce metastases. The absence of lymph node and macroscopic pulmonary metastases, and the preservation of basal lamina integrity in the microscopic tumors detected in Ad-CX3CL1–treated mice indicate that Ad-CX3CL1 fosters development of neoplastic lesions rather than metastatic dissemination of the injected tumor. This idea is reinforced by the dose-dependent effect of Ad-CX3CL1 treatment on tumor multiplicity. Damage to the tumor vasculature during injection could facilitate systemic virus dissemination (43), enabling the infection of distal mammary glands. In addition, CX3CL1 can be cleaved from the membrane of Ad–CX3CL1–transduced cells, leading to increased serum CX3CL1 levels.

The second line of evidence is the significant delay in the onset of spontaneous mammary tumors and the reduction in tumor multiplicity in Tg-neu-CX3CL1$^{-/-}$ and hemizygous Tg-neu-CX3CL1$^{+/-}$ mice compared with WT littermates. The growth kinetics of established tumors was nonetheless unaffected by CX3CL1 deficiency, which concurs with the lack of Ad-CX3CL1 effect on tumor growth. These data suggest that in this model, CX3CL1 promoter activity takes place in early stages of carcinogenesis.

Tumor multiplicity is not comparable between Ad-LacZ–injected (Fig. 3J) and noninjected Tg-neu mice (Fig. 6B); this could be a consequence of an injury reaction due to repeated intratumor injection of adenovirus. Such a response could reactivate a low-affinity, neu-specific T-cell repertoire in Tg-neu mice (24), thus partially restricting tumor growth. This reaction, which would be similar in Ad-LacZ- and Ad-CX3CL1–injected mice, would not occur in noninjected Tg-neu mice.

The mechanism by which CX3CL1 enhances mammary carcinogenesis in Tg-neu mice is not entirely clear. Although CX3CL1 is a proinflammatory chemokine that might promote tumorigenesis by fostering inflammation, histologic analyses showed no marked changes in the inflammatory infiltrate associated with CX3CL1 overexpression or deficiency in Tg-neu tumors. Our *in vitro* results using human breast cancer lines and primary mammary epithelial cells from Tg-neu mice indicate that CX3CL1 enhances cell proliferation by transactivating ErbB receptors. Moreover, CX3CL1 deficiency does not affect tumor onset or multiplicity in Tg-PyMT mice, thus associating CX3CL1-mediated stimulation of mammary carcinogenesis with ErbB2 overexpression and signaling. CX3CR1-ErbB crosstalk is probably not involved in tumor initiation; most mammary tumors in Tg-neu mice have in-frame deletions and insertions of cysteine residues in the ErbB2 extracellular domain, which leads to constitutive receptor dimerization and activation (40).

Accumulated evidence indicates bidirectional cross-communication between GPCR, the family to which CX3CR1 belongs, and RTK such as ErbB receptors (18, 21, 42). Although this crosstalk might take place exclusively through intracellular signaling circuits, GPCR

usually induce RTK transactivation through an extracellular mechanism involving proteolytic release of the RTK ligand, which binds to and activates the receptor (17, 18). This "triple passing membrane" signaling usually leads to MAPK pathway activation (18). The blockade of CX3CL1-mediated cell proliferation and of ERK activation in T47D cells by a general MMP inhibitor indicates that CX3CL1/ ErbB crosstalk is controlled by ErbB ligand release from the cell membrane. The specific ligand involved in the transactivation circuit might depend on cell type; for instance, blockade of HB-EGF, amphiregulin, or TGFα inhibited CX3CL1-induced ERK activation in T47D cells.

Analysis of CX3CL1-triggered signaling pathways in breast tumors suggested that ErbB transactivation was specifically needed for CX3CL1-mediated ERK activation, which was unaffected by PTx, but was impaired by the general MMP inhibitor. The ERK pathway induces transcription and secretion of several ErbB ligands (44), which could create a positive feedback loop that fosters tumor progression. In contrast to ERK, PI3K pathway activation was MMP-independent, suggesting that ErbB transactivation was not involved. In addition, PTx did not inhibit AKT phosphorylation, implying that PI3K activation is $G\alpha_i$-independent in T47D cells. In smooth muscle cells, CX3CL1-induced ErbB transactivation is implicated in PI3K, but not in ERK activation (22).

We thus propose a model in which CX3CL1 accelerates the development of incipient neoplastic lesions by enhancing the ERK pathway through ErbB transactivation (Fig. 7). Such crosstalk would not operate in Tg-PyMT mice, as membrane-bound PyMT directly triggers PI3K and ERK signaling pathways after c-SRC binding and activation (45); this would render PyMT-expressing cells independent of CX3CL1 and ErbB, although PyMT can induce ErbB2 upregulation. The CX3CL1/ErbB crosstalk would be operative, even though Tg-neu tumors express a constitutively activated ErbB2 receptor. Indeed, overexpression of hypofunctional ErbB1 delays mammary tumor onset in MMTV-neu[NDL] mice, which express an oncogenic form of ErbB2 (46); the delayed latency of these tumors correlates with lower phosphorylation of GAB1, an adapter protein involved in ERK signaling (47). It is tempting to speculate that CX3CL1-induced transactivation causes qualitative and quantitative changes in the strength, frequency, and/or adaptation of ERK signaling in transformed mammary cells, conferring a proliferative advantage. Some studies indicate that these ERK signaling parameters affect cell fate decisions (16, 48).

In summary, we show that CX3CL1 acts as a tumor promoter for the development of spontaneous mouse mammary carcinomas, in models in which ErbB signaling is relevant for tumorigenesis. Our results also highlight the importance of the GPCR–RTK crosstalk in early stages of breast carcinogenesis, which might be extensible to other cancer types (49). As the *erbB2* gene is amplified in approximately 30% of human breast tumors, and approximately 50% of breast cancers overexpress EGFR and EGFRvIII receptors (15, 50), we propose that the CX3CL1-induced ErbB transactivation reported here operates in human breast cancers, the most common malignancy among women worldwide.

Supplementary Material

Refer to Web version on PubMed Central for supplementary material.

Acknowledgments

References

1. Boudreau A, van 't Veer LJ, Bissell MJ. An "elite hacker": breast tumors exploit the normal microenvironment program to instruct their progression and biological diversity. Cell Adh Migr. 2012; 6:236–248. [PubMed: 22863741]

2. Balkwill FR. The chemokine system and cancer. J Pathol. 2012; 226:148–157. [PubMed: 21989643]

3. DeNardo DG, Andreu P, Coussens LM. Interactions between lymphocytes and myeloid cells regulate pro- versus anti-tumor immunity. Cancer Metastasis Rev. 2010; 29:309–316. [PubMed: 20405169]

4. Conforti R, Ma Y, Morel Y, Paturel C, Terme M, Viaud S, et al. Opposing effects of toll-like receptor (TLR3) signaling in tumors can be therapeutically uncoupled to optimize the anticancer efficacy of TLR3 ligands. Cancer Res. 2010; 70:490–500. [PubMed: 20068181]

5. González-Martín A, Mira E, Mañes S. CCR5 as a potential target in cancer therapy: inhibition or stimulation? Anticancer Agents Med Chem. 2012; 12:1045–1057. [PubMed: 22583417]

6. Acosta JC, O'Loghlen A, Banito A, Guijarro MV, Augert A, Raguz S, et al. Chemokine signaling via the CXCR2 receptor reinforces senescence. Cell. 2008; 133:1006–1018. [PubMed: 18555777]

7. Mañes S, Mira E, Colomer R, Montero S, Real LM, Gómez-Moutón C, et al. CCR5 expression influences the progression of human breast cancer in a p53-dependent manner. J Exp Med. 2003; 198:1381–1389. [PubMed: 14597737]

8. Erreni M, Solinas G, Brescia P, Osti D, Zunino F, Colombo P, et al. Human glioblastoma tumours and neural cancer stem cells express the chemokine CX3CL1 and its receptor CX3CR1. Eur J Cancer. 2010; 46:3383–3392. [PubMed: 20728344]

9. Gaudin F, Nasreddine S, Donnadieu AC, Emilie D, Combadière C, Prévot S, et al. Identification of the chemokine CX3CL1 as a new regulator of malignant cell proliferation in epithelial ovarian cancer. PLoS ONE. 2011; 6:e21546. [PubMed: 21750716]

10. Jamieson WL, Shimizu S, D'Ambrosio JA, Meucci O, Fatatis A. CX3CR1 is expressed by prostate epithelial cells and androgens regulate the levels of CX3CL1/fractalkine in the bone marrow: potential role in prostate cancer bone tropism. Cancer Res. 2008; 68:1715–1722. [PubMed: 18339851]

11. Shiraishi K, Fukuda S, Mori T, Matsuda K, Yamaguchi T, Tanikawa C, et al. Identification of fractalkine, a CX3C–type chemokine, as a direct target of p53. Cancer Res. 2000; 60:3722–3726. [PubMed: 10919640]

12. Guo J, Zhang M, Wang B, Yuan Z, Guo Z, Chen T, et al. Fractalkine transgene induces T-cell-dependent antitumor immunity through chemoattraction and activation of dendritic cells. Int J Cancer. 2003; 103:212–220. [PubMed: 12455035]

13. Lavergne E, Combadiere B, Bonduelle O, Iga M, Gao JL, Maho M, et al. Fractalkine mediates natural killer-dependent antitumor responses *in vivo*. Cancer Res. 2003; 63:7468–7474. [PubMed: 14612547]

14. Tang L, Hu HD, Hu P, Lan YH, Peng ML, Chen M, et al. Gene therapy with CX3CL1/Fractalkine induces antitumor immunity to regress effectively mouse hepatocellular carcinoma. Gene Ther. 2007; 14:1226–1234. [PubMed: 17597794]

15. Arribas J, Baselga J, Pedersen K, Parra-Palau JL. p95HER2 and breast cancer. Cancer Res. 2011; 71:1515–1519. [PubMed: 21343397]

16. Avraham R, Yarden Y. Feedback regulation of EGFR signalling: decision making by early and delayed loops. Nat Rev Mol Cell Biol. 2011; 12:104–117. [PubMed: 21252999]

17. Fischer OM, Hart S, Gschwind A, Ullrich A. EGFR signal transactivation in cancer cells. Biochem Soc Trans. 2003; 31:1203–1208. [PubMed: 14641026]

18. Liebmann C. EGF receptor activation by GPCRs: an universal pathway reveals different versions. Mol Cell Endocrinol. 2011; 331:222–231. [PubMed: 20398727]

19. Biscardi JS, Maa MC, Tice DA, Cox ME, Leu TH, Parsons SJ. c-Src-mediated phosphorylation of the epidermal growth factor receptor on Tyr845 and Tyr1101 is associated with modulation of receptor function. J Biol Chem. 1999; 274:8335–8343. [PubMed: 10075741]

20. Zwang Y, Yarden Y. p38 MAP kinase mediates stress-induced internalization of EGFR: implications for cancer chemotherapy. EMBO J. 2006; 25:4195–4206. [PubMed: 16932740]

21. Prenzel N, Zwick E, Daub H, Leserer M, Abraham R, Wallasch C, et al. EGF receptor transactivation by G-protein-coupled receptors requires metalloproteinase cleavage of proHB-EGF. Nature. 1999; 402:884–888. [PubMed: 10622253]

22. White GE, Tan TC, John AE, Whatling C, McPheat WL, Greaves DR. Fractalkine has anti-apoptotic and proliferative effects on human vascular smooth muscle cells via epidermal growth factor receptor signalling. Cardiovasc Res. 2010; 85:825–835. [PubMed: 19840952]

23. Cook DN, Chen SC, Sullivan LM, Manfra DJ, Wiekowski MT, Prosser DM, et al. Generation and analysis of mice lacking the chemokine fractalkine. Mol Cell Biol. 2001; 21:3159–3165. [PubMed: 11287620]

24. González-Martín A, Gómez L, Lustgarten J, Mira E, Mañs S. Maximal T cell-mediated antitumor responses rely upon CCR5 expression in both CD4(+)and CD8(+) T cells. Cancer Res. 2011; 71:5455–5466. [PubMed: 21715565]

25. Stingl J, Eirew P, Ricketson I, Shackleton M, Vaillant F, Choi D, et al. Purification and unique properties of mammary epithelial stem cells. Nature. 2006; 439:993–997. [PubMed: 16395311]

26. Alvarez-Diaz S, Valle N, Garcia JM, Peña C, Freije JM, Quesada V, et al. Cystatin D is a candidate tumor suppressor gene induced by vitamin D in human colon cancer cells. J Clin Invest. 2009; 119:2343–2358. [PubMed: 19662683]

27. Lacalle RA, Peregil RM, Albar JP, Merino E, Martínez AC, Mérida I, et al. Type I phosphatidylinositol 4-phosphate 5-kinase controls neutrophil polarity and directional movement. J Cell Biol. 2007; 179:1539–1553. [PubMed: 18158329]

28. Sleeman KE, Kendrick H, Ashworth A, Isacke CM, Smalley MJ. CD24 staining of mouse mammary gland cells defines luminal epithelial, myoepithelial/basal and non-epithelial cells. Breast Cancer Res. 2006; 8:R7. [PubMed: 16417656]

29. Richardson AL, Wang ZC, De Nicolo A, Lu X, Brown M, Miron A, et al. X chromosomal abnormalities in basal-like human breast cancer. Cancer Cell. 2006; 9:121–132. [PubMed: 16473279]

30. Casey T, Bond J, Tighe S, Hunter T, Lintault L, Patel O, et al. Molecular signatures suggest a major role for stromal cells in development of invasive breast cancer. Breast Cancer Res Treat. 2009; 114:47–62. [PubMed: 18373191]

31. Chen DT, Nasir A, Culhane A, Venkataramu C, Fulp W, Rubio R, et al. Proliferative genes dominate malignancy-risk gene signature in histologically-normal breast tissue. Breast Cancer Res Treat. 2010; 119:335–346. [PubMed: 19266279]

32. Vitale S, Cambien B, Karimdjee BF, Barthel R, Staccini P, Luci C, et al. Tissue-specific differential antitumour effect of molecular forms of fractalkine in a mouse model of metastatic colon cancer. Gut. 2007; 56:365–372. [PubMed: 16870716]

33. Cardona AE, Pioro EP, Sasse ME, Kostenko V, Cardona SM, Dijkstra IM, et al. Control of microglial neurotoxicity by the fractalkine receptor. Nat Neurosci. 2006; 9:917–924. [PubMed: 16732273]

34. Kim KW, Vallon-Eberhard A, Zigmond E, Farache J, Shezen E, Shakhar G, et al. *In vivo* structure/function and expression analysis of the CX3C chemokine fractalkine. Blood. 2011; 118:e156–e167. [PubMed: 21951685]

35. Neve RM, Chin K, Fridlyand J, Yeh J, Baehner FL, Fevr T, et al. A collection of breast cancer cell lines for the study of functionally distinct cancer subtypes. Cancer Cell. 2006; 10:515–527. [PubMed: 17157791]

36. Drasin DJ, Robin TP, Ford HL. Breast cancer epithelial-to-mesenchymal transition: examining the functional consequences of plasticity. Breast Cancer Res. 2011; 13:226. [PubMed: 22078097]

37. Casas E, Kim J, Bendesky A, Ohno-Machado L, Wolfe CJ, Yang J. Snail2 is an essential mediator of Twist1-induced epithelial mesenchymal transition and metastasis. Cancer Res. 2011; 71:245–254. [PubMed: 21199805]

38. Harrell JC, Dye WW, Allred DC, Jedlicka P, Spoelstra NS, Sartorius CA, et al. Estrogen receptor positive breast cancer metastasis: altered hormonal sensitivity and tumor aggressiveness in lymphatic vessels and lymph nodes. Cancer Res. 2006; 66:9308–9315. [PubMed: 16982776]

39. Vasudevan KM, Barbie DA, Davies MA, Rabinovsky R, McNear CJ, Kim JJ, et al. AKT-independent signaling downstream of oncogenic PIK3CA mutations in human cancer. Cancer Cell. 2009; 16:21–32. [PubMed: 19573809]

40. Ursini-Siegel J, Schade B, Cardiff RD, Muller WJ. Insights from transgenic mouse models of ERBB2-induced breast cancer. Nat Rev Cancer. 2007; 7:389–397. [PubMed: 17446858]

41. Marcotte R, Muller WJ. Signal transduction in transgenic mouse models of human breast cancer–implications for human breast cancer. J Mammary Gland Biol Neoplasia. 2008; 13:323–335. [PubMed: 18651209]

42. Mira E, Lacalle RA, Gonzalez MA, Gomez-Mouton C, Abad JL, Bernad A, et al. A role for chemokine receptor transactivation in growth factor signaling. EMBO Rep. 2001; 2:151–156. [PubMed: 11258708]

43. Wang Y, Hu JK, Krol A, Li YP, Li CY, Yuan F. Systemic dissemination of viral vectors during intratumoral injection. Mol Cancer Ther. 2003; 2:1233–1242. [PubMed: 14617797]

44. Schulze A, Lehmann K, Jefferies HB, McMahon M, Downward J. Analysis of the transcriptional program induced by Raf in epithelial cells. Genes Dev. 2001; 15:981–994. [PubMed: 11316792]

45. Rodriguez-Viciana P, Collins C, Fried M. Polyoma and SV40 proteins differentially regulate PP2A to activate distinct cellular signaling pathways involved in growth control. Proc Natl Acad Sci USA. 2006; 103:19290–19295. [PubMed: 17158797]

46. Gillgrass A, Cardiff RD, Sharan N, Kannan S, Muller WJ. Epidermal growth factor receptor-dependent activation of Gab1 is involved in ErbB-2-mediated mammary tumor progression. Oncogene. 2003; 22:9151–9155. [PubMed: 14668796]

47. Takahashi-Tezuka M, Yoshida Y, Fukada T, Ohtani T, Yamanaka Y, Nishida K, et al. Gab1 acts as an adapter molecule linking the cytokine receptor gp130 to ERK mitogen-activated protein kinase. Mol Cell Biol. 1998; 18:4109–4117. [PubMed: 9632795]

48. von Kriegsheim A, Baiocchi D, Birtwistle M, Sumpton D, Bienvenut W, Morrice N, et al. Cell fate decisions are specified by the dynamic ERK interactome. Nat Cell Biol. 2009; 11:1458–1464. [PubMed: 19935650]

49. Bongers G, Muniz LR, Pacer ME, Iuga AC, Thirunarayanan N, Slinger E, et al. A role for the epidermal growth factor receptor signaling in development of intestinal serrated polyps in mice and humans. Gastroenterology. 2012; 143:730–740. [PubMed: 22643351]

50. Rae JM, Scheys JO, Clark KM, Chadwick RB, Kiefer MC, Lippman ME. EGFR and EGFRvIII expression in primary breast cancer and cell lines. Breast Cancer Res Treat. 2004; 87:87–95. [PubMed: 15377854]
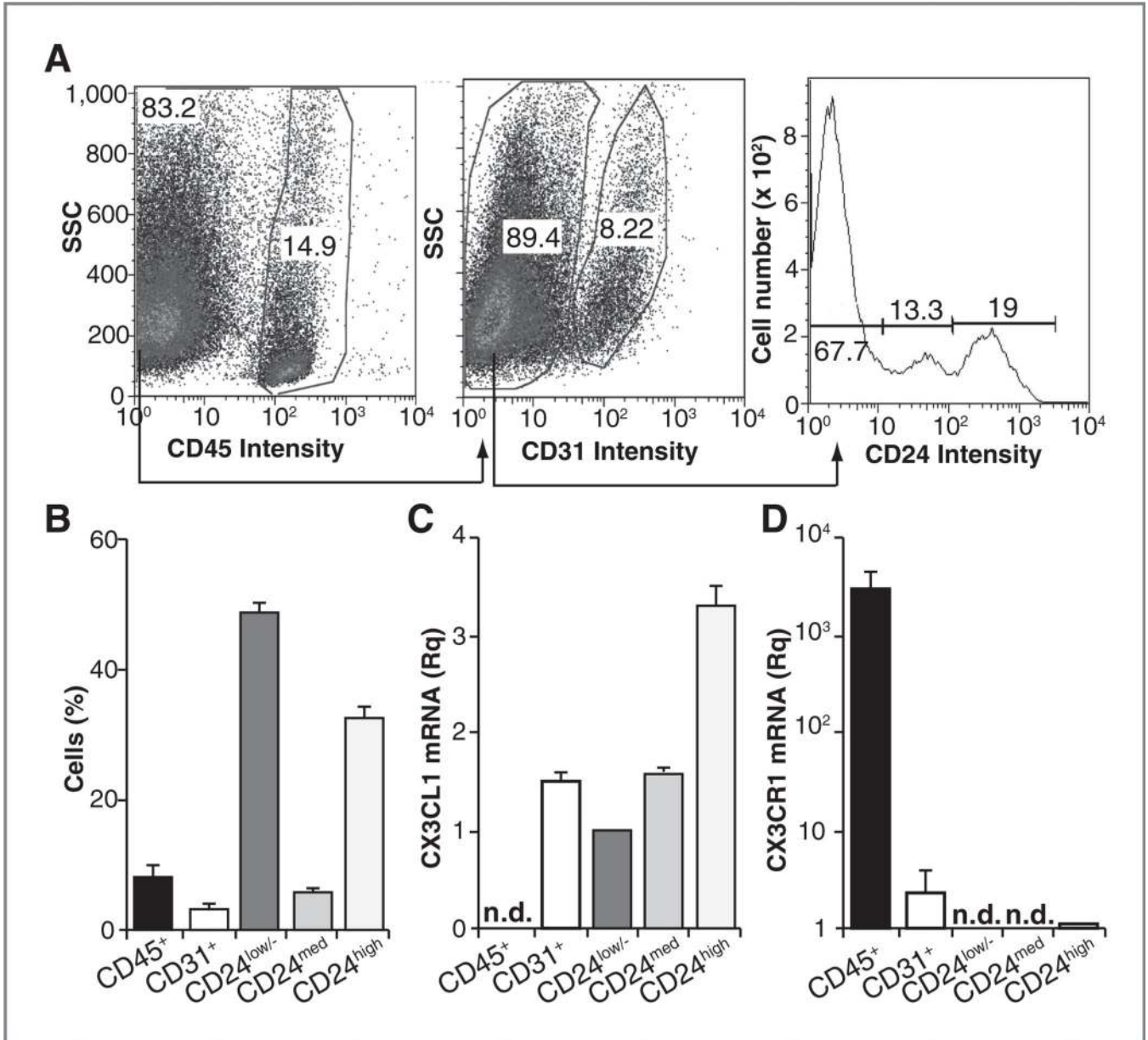
Figure 1.
CX3CL1 is expressed in specific cell types in the mouse mammary gland. Analysis of cell types composing nontumor mammary glands. A, fluorescence-activated cell sorting analysis of a representative purification experiment. B, graph summarizing the percentage of each cell type; data are mean ± SEM in 3 independent experiments ($n = 32$ glands each). C and D, relative expression of CX3CL1 (C) and CX3CR1 (D) mRNA in the cell subtypes. Data are mean ± SEM of the relative quantity ($2^{-\Delta\Delta Ct}$), using as reference the sample with the highest C_t value for each mRNA after normalization to β-actin ($n = 3$). n.d., not detected ($C_t = 40$).
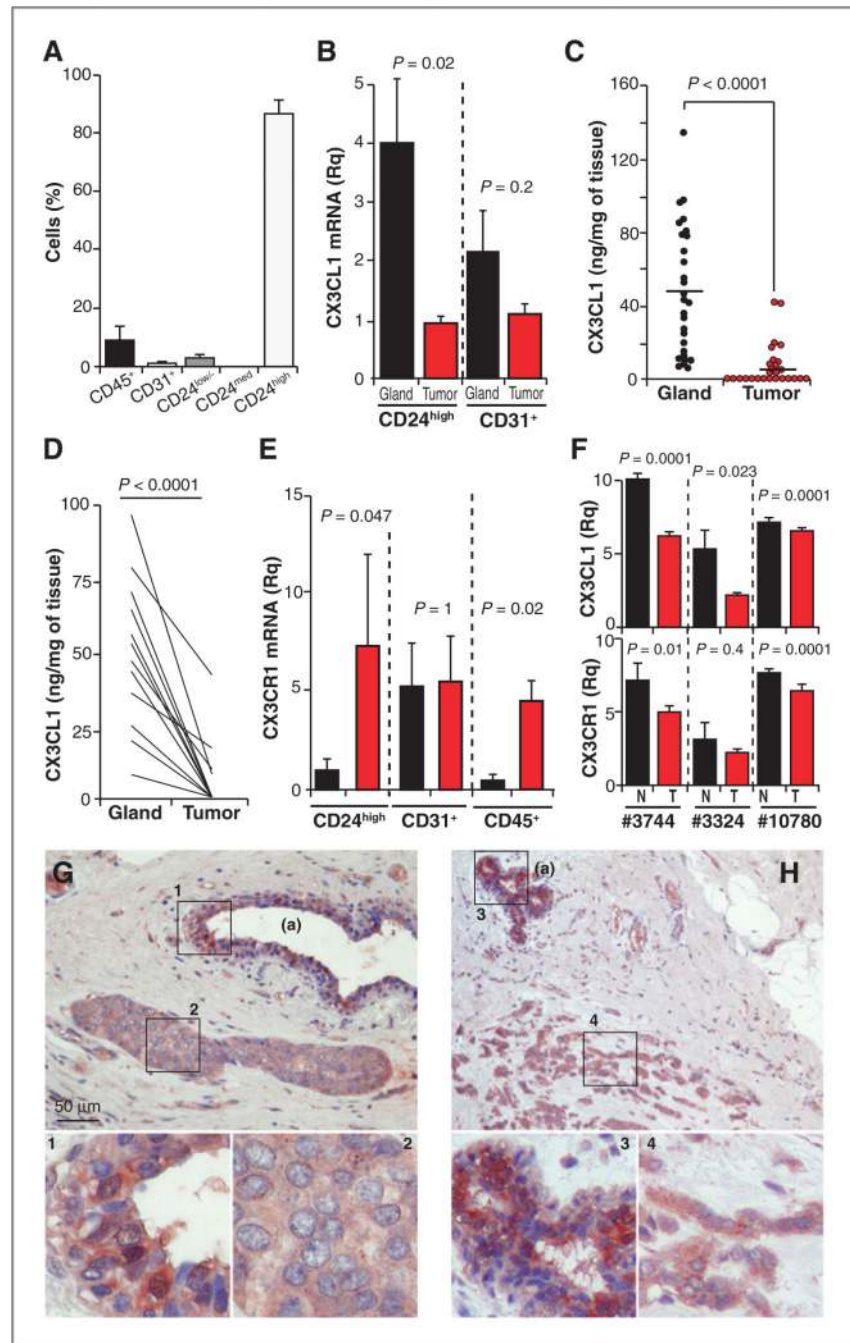
Figure 2.
CX3CL1 is downmodulated in breast tumors compared with healthy breast tissue. A, relative proportion of cell types in Tg-neu tumors; data are mean ± SEM ($n = 6$). B, relative quantity of CX3CL1 mRNA in epithelial (CD24^{high}) and endothelial cells isolated from tumors and normal breasts; data are mean ± SEM ($n = 3$, nontumor; $n = 6$, tumors; Mann–Whitney test). C, CX3CL1 levels in total extracts from normal glands and breast tumors determined by ELISA ($n = 28$); each point is the mean of triplicates from at least two independent assays (two-tailed Student t test). D, CX3CL1 protein amounts for paired

nontumor and tumor samples as in C. E, relative quantity of CX3CR1 mRNA in the indicated cell types isolated from tumors and normal glands as in B. F, relative expression of CX3CL1 and CX3CR1 mRNA in human breast tumors and normal tissue; data derived from GEOprofile Database. For B, E, and F, data were compared using the Mann–Whitney *U* test; normal breast tissue (black), tumors (red). G and H, CX3CL1 staining of representative *in situ* (G) and invasive (H) human ductal carcinomas (*n* = 4); adjacent nontumor breast tissue (a) is also indicated. Higher magnification insets are also shown. Fisher two-tailed test to compare tumor and normal tissue, *P* = 0.0286.
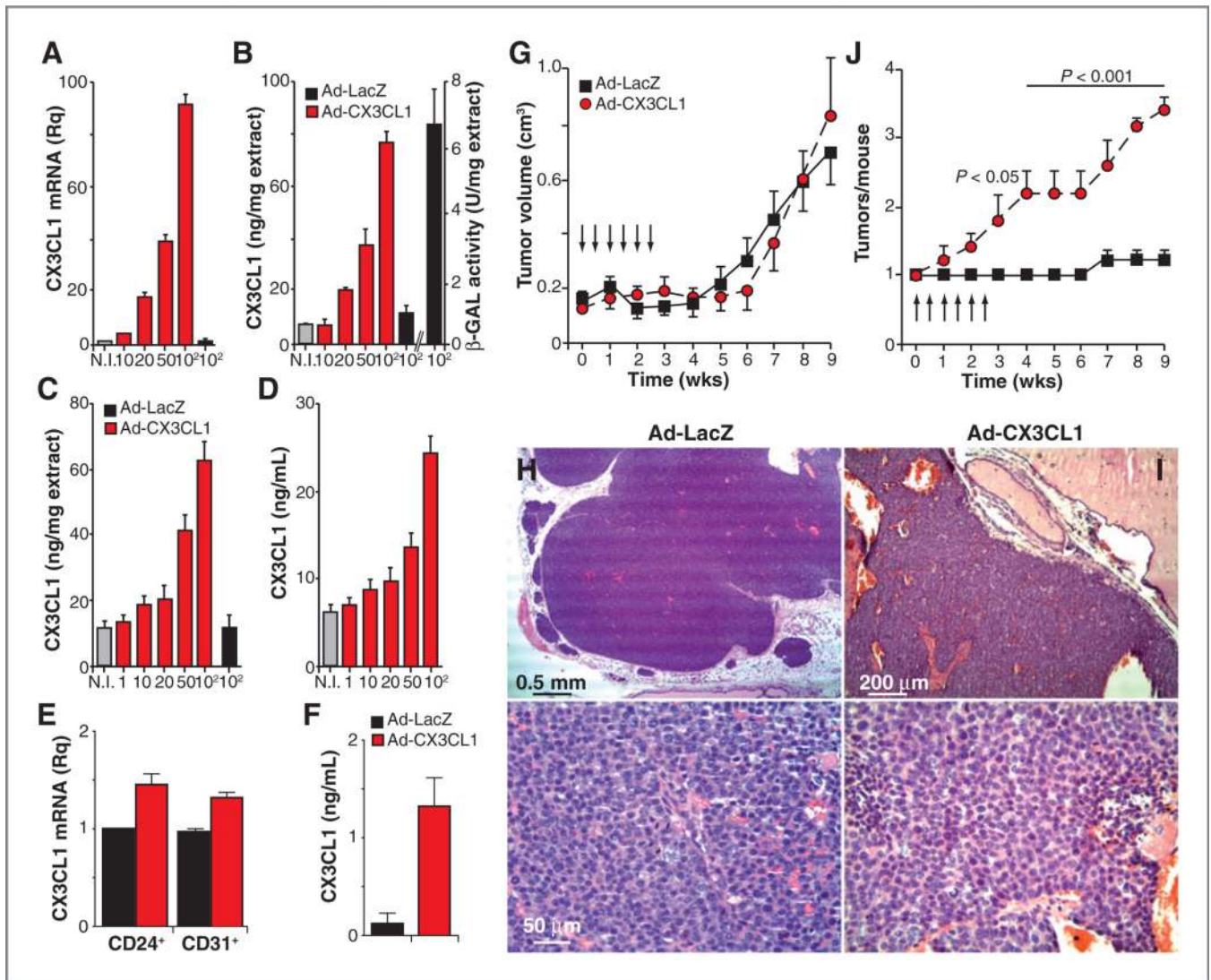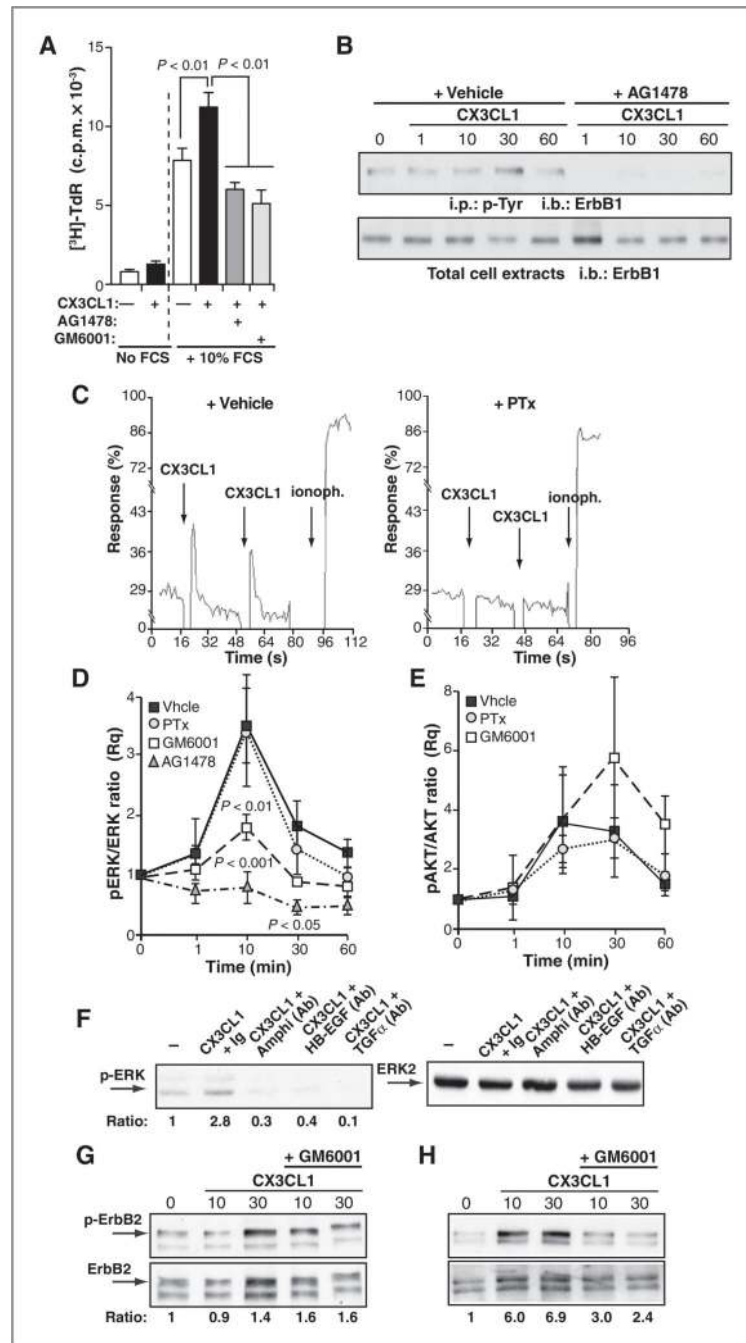
Figure 3.
CX3CL1 over-expression increases breast carcinogenesis in Tg-neu mice. A, relative CX3CL1 mRNA expression in uninfected (NI), Ad-CX3CL1-, and Ad-LacZ–infected N202.1A cells (MOI indicated). B, ELISA determination of CX3CL1 levels in extracts of N202.1A cells as in A; β-galactosidase (β-GAL) activity in extracts of Ad-LacZ–infected cells is shown as control. C and D, ELISA determination of CX3CL1 levels in extracts (C) and conditioned medium (D) of Ad-CX3CL1- and Ad-LacZ-infected 1g11 cells. For A-D, data are mean ± SEM of triplicates in one representative experiment of two carried out. E, CX3CL1 mRNA levels in cell populations isolated from Tg-neu tumors after intratumor Ad-CX3CL1 injection. F, CX3CL1 serum levels in mice as in E; n = 3 mice/group. G, tumor growth kinetics in Tg-neu mice after intratumoral injections (arrows) of Ad-CX3CL1 or Ad-LacZ viruses. H and I, hematoxylin and eosin-stained sections of formalin-fixed tumors inoculated with Ad-CX3CL1 or Ad-LacZ. Representative images are shown (n = 3 tumors/group). J, mean tumor number in Tg-neu mice as in G. For G and J, data are mean ± SEM (n = 5 mice/group; two-way ANOVA with Bonferroni posttest).
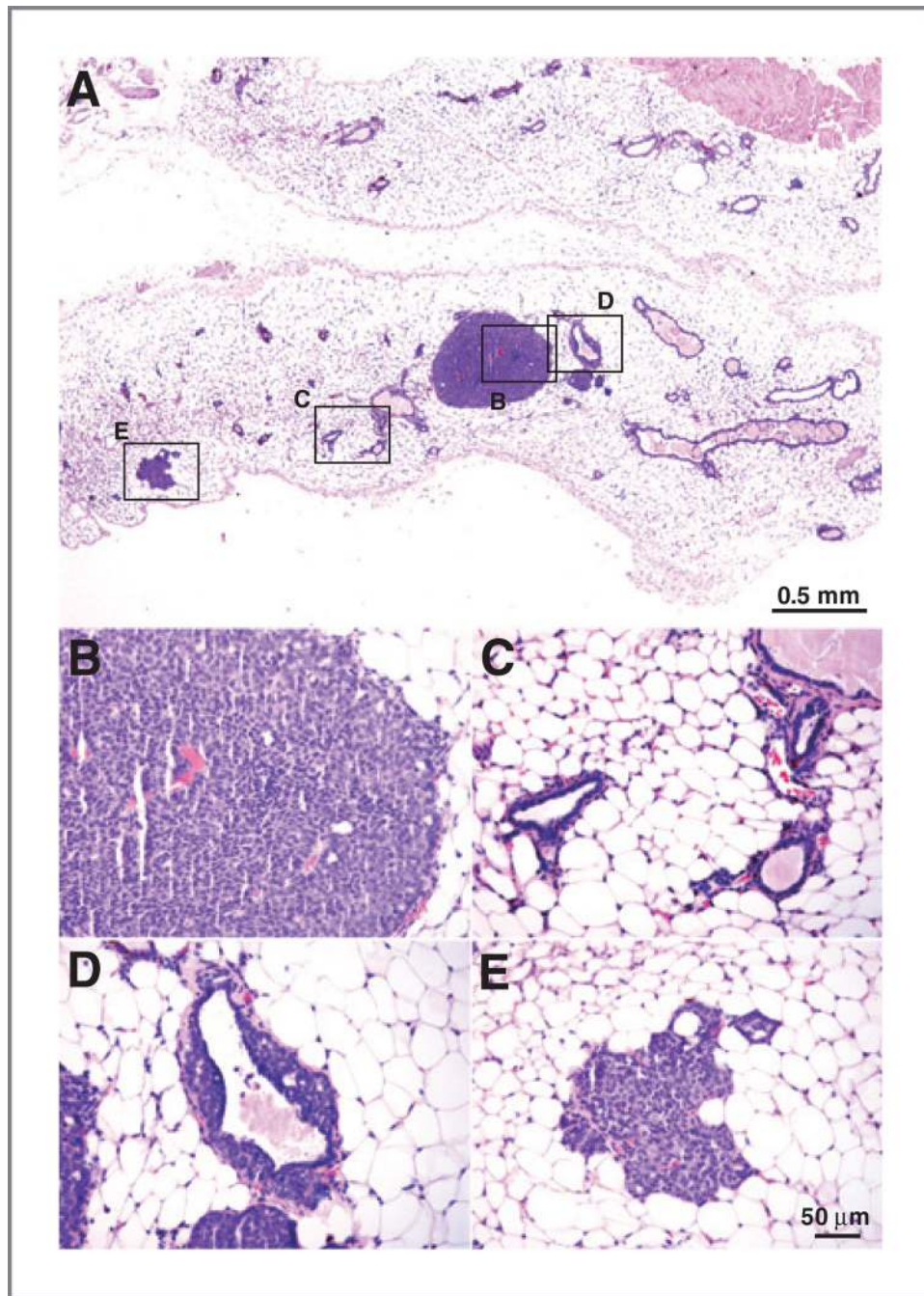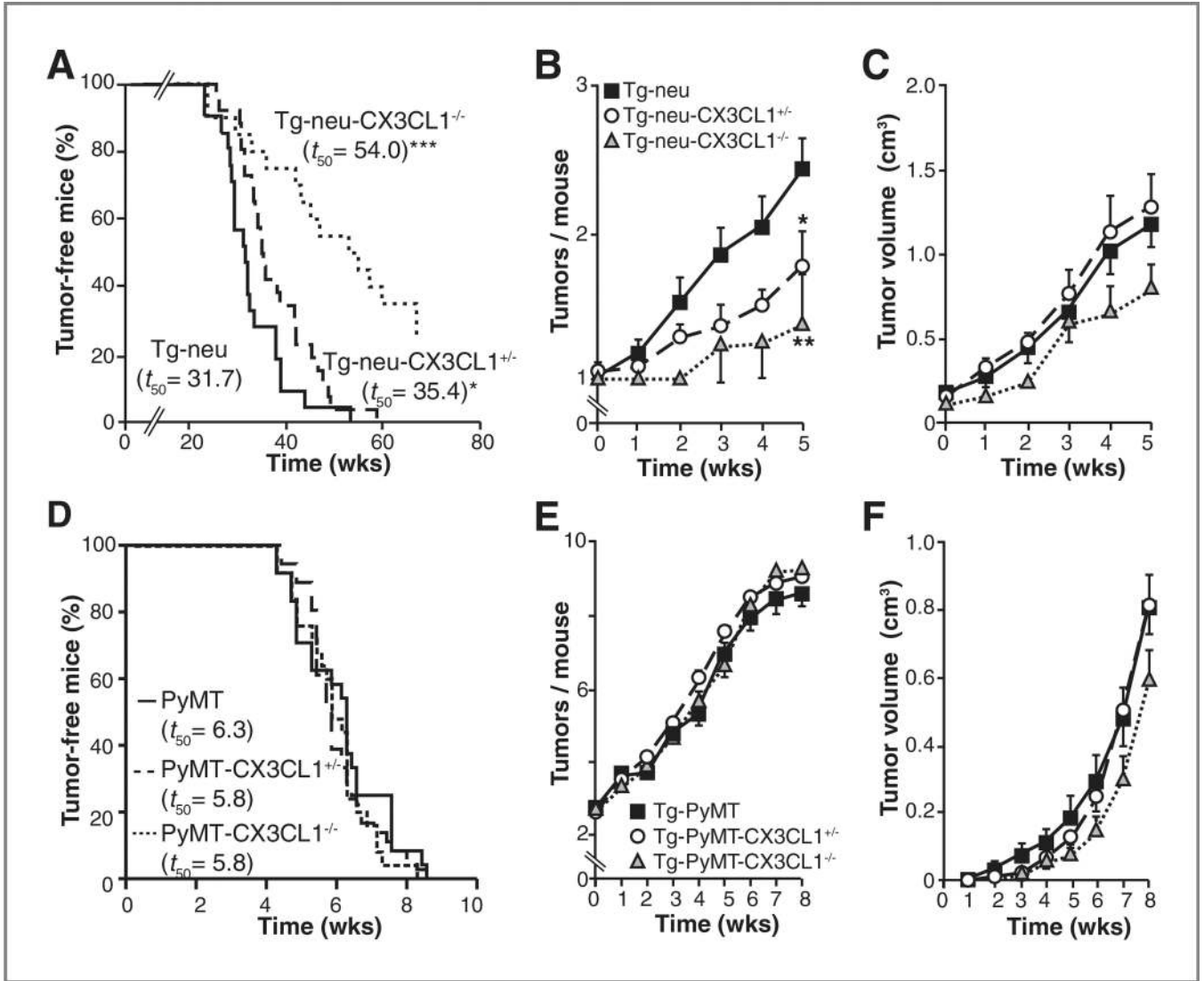
Figure 4.
Detection of microtumors in Ad-CX3CL1–treated mice. A, panoramic view of hematoxylin and eosin-stained mammary glands without macroscopic tumors from an Ad-CX3CL1–injected mouse. Selected areas are shown at higher magnification in tumor mass (B), normal glands (C), and glands with intraductal epithelial proliferation (D). E, some glands distant from the tumor showed characteristics similar to the hyperplastic foci described above.

Figure 5.
CX3CL1 induces transactivation of the EGF pathway in tumors and breast epithelial cells.
A, [^{3}H]-TdR incorporation in T47D cells, unstimulated (−) or stimulated with CX3CL1,
with or without FCS and the indicated inhibitors. Data are mean ± SEM counts per minute
(c.p.m.) from octuplicates in a representative experiment ($n = 2$ without FCS; $n = 5$ with
FCS; one-way ANOVA, Dunnett posttest). B, CX3CL1-induced tyrosine phosphorylation of
ErbB1 in T47D cells stimulated with the chemokine for the indicated times, alone or with
AG1478. Cell extracts were precipitated with anti-phosphotyrosine (p-Tyr) antibody (top) or

directly resolved by SDS-PAGE and blotted with anti-ErbB1 (bottom); a representative experiment of two is shown. C, CX3CL1-induced Ca^{2+} flux in vehicle- or PTx-treated T47D cells loaded with Fluo-3, AM ($n = 2$). D and E, analysis of CX3CL1-induced ERK (D) and AKT (E) activation in T47D cells pretreated with inhibitors and stimulated with CX3CL1 for indicated times. Phosphorylated ERK 1/2 and AKT and total ERK and AKT were determined in cell extracts. pERK/ ERK (D) and pAKT/AKT (E) ratios were calculated by densitometry and normalized to unstimulated conditions. Data are mean ± SEM ($n = 4$; two-way ANOVA with Bonferroni posttest). F, blockade of CX3CL1-induced ERK phosphorylation by neutralizing antibodies to the indicated ErbB ligands. Numbers (bottom) indicate the pERK/ERK ratio for each condition. G and H, analysis of CX3CL1-induced ErbB2 phosphorylation in primary cultures of Tg-neu tumors (G) or mammary epithelial cells (H). Representative blots of CX3CL1-stimulated tumors or breast epithelial cells, alone or with GM6001 ($n = 2$, tumors; $n = 3$, normal epithelium). Numbers (bottom) indicate the pErbB2/ ErbB2 ratio for each condition. i.p., immunoprecipitation; i.b., immunoblotting.

Figure 6.
CX3CL1 deficiency specifically delays breast carcinogenesis in Tg-neu mice. A, Kaplan-Meier plots showing the percentage of tumor-free, virgin female Tg-neu ($n = 21$), Tg-neu-CX3CL1$^{+/-}$ ($n = 26$), and Tg-neu-CX3CL1$^{-/-}$ ($n = 20$) mice as a function of postnatal age (*$P = 0.04$; ***$P < 0.0001$; log-rank Test). B, number of palpable breast tumors per mouse (mean ± SEM) in Tg-neu ($n = 22$), Tg-neu-CX3CL1$^{+/-}$ ($n = 21$) and Tg-neu-CX3CL1$^{-/-}$ ($n = 8$) mice (*$P < 0.05$; **$P < 0.01$; two-way Anova with Bonferroni post-test). C, growth of spontaneous tumors in mice in A was analyzed by weekly measurement for 5 weeks. D, CX3CL1 deficiency does not delay breast carcinogenesis in Tg-PyMT mice. Kaplan-Meier plots showing the percentage of tumor-free, virgin female Tg-PyMT($n = 24$), Tg-PyMT-CX3CL1$^{+/-}$ ($n = 32$), and Tg-PyMT-CX3CL1$^{-/-}$ ($n = 19$) mice as a function of postnatal age. E and F, mean number of tumors per mice (E) and growth kinetics (F) of breast tumors that arose in mice n D. Data are mean ± SEM.
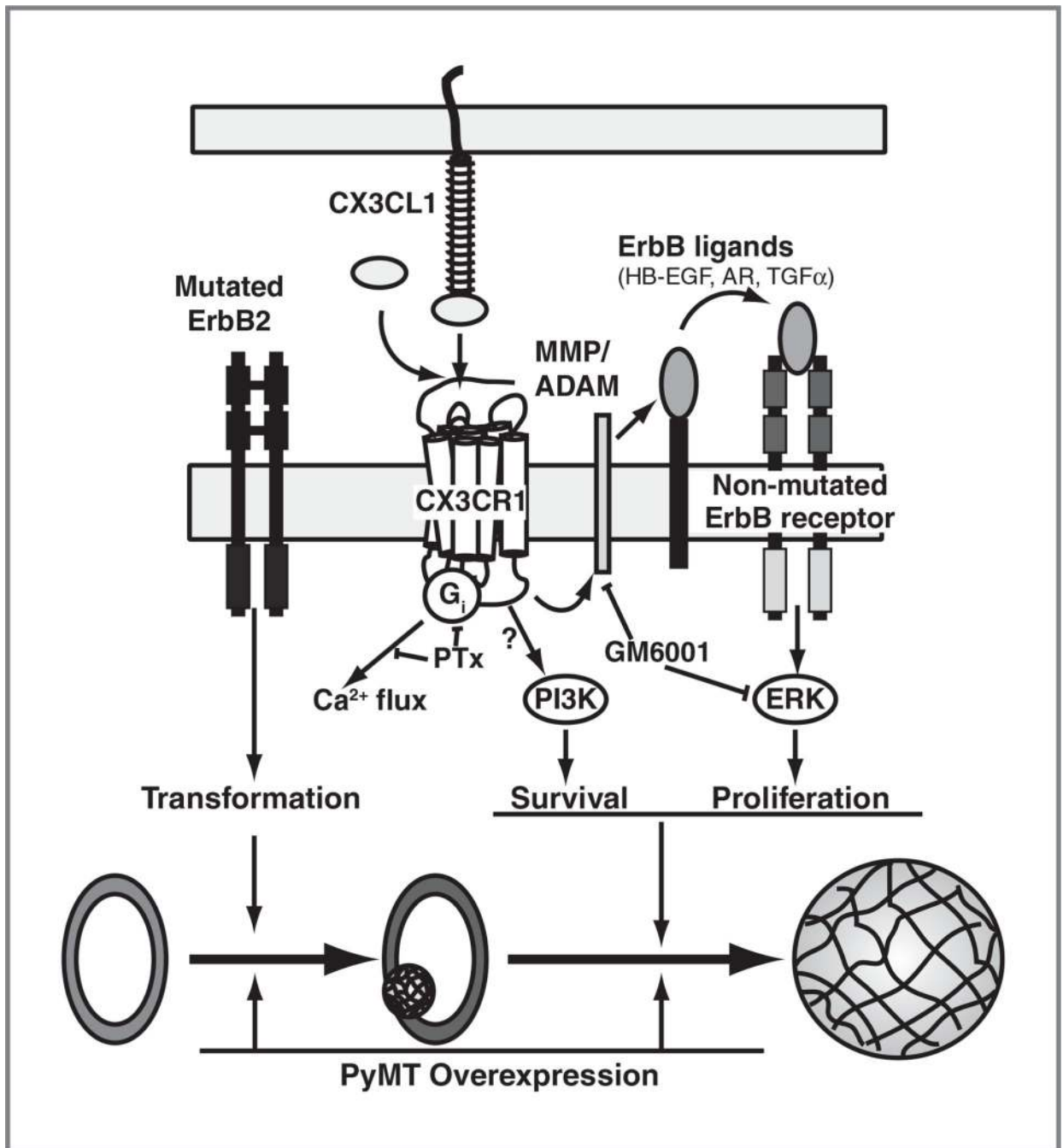
Figure 7.
Model of CX3CL1-induced breast carcinogenesis in ErbB2 transgenic mice. We propose that CX3CL1 is not involved in tumor initiation, which is probably mediated by ErbB2 mutagenesis. In this model, CX3CL1 would promote the progression of small or preneoplastic lesions in the mammary gland by enhancing ERK pathway activation through transactivation of the ErbB receptor family. Direct activation of this mitogenic pathway by PyMT would overcome the effect of CX3CL1 on breast tumorigenesis in Tg-PyMT mice.

HB-EGF, heparin-binding EGF; AR, amphiregulin, ADAM, a disintegrin and metalloprotease.